Microbiology[1]

Kelemen, P.B., Matter, J.M., Teagle, D.A.H., Coggon, J.A., and the Oman Drilling Project Science Team[2]

Keywords: Oman Drilling Project, OmanDP, Samail ophiolite, Site GT3, Site BT1, Site BA1, Site BA2, Site BA3, Site BA4, microbiology, well chips, drill cuttings, DNA, RNA, lipids, cell cultivation, bulk nitrogen

Chapter contents

Microbiology sampling 1
Results 2
References 7
Figures 8

[1]Kelemen, P.B., Matter, J.M., Teagle, D.A.H., Coggon, J.A., and the Oman Drilling Project Science Team, 2021. Microbiology. *In* Kelemen, P.B., Matter, J.M., Teagle, D.A.H., Coggon, J.A., and the Oman Drilling Project Science Team, *Proceedings of the Oman Drilling Project*: College Station, TX (International Ocean Discovery Program). https://doi.org/10.14379/OmanDP.proc.2020
[2]**OmanDP Science Team affiliations.**

MS OmanDP-119
Published 6 April 2021

Microbiology sampling

Hole GT3A

A whole-round gabbro sample was collected from Core 131Z in Hole GT3A for DNA/RNA and lipid extractions. Samples were taken from the inside and outside of the core, as well as water from the rock saw used to cut the core.

- 3 replicates from inside of core (~0.25–0.5 g crushed rock).
- 3 replicates from outside of core (~0.25–0.5 g crushed rock).
- 3 replicates of ~5 mL of water from the rock saw used to cut the core interval.
- 3 replicates of both inner and outer core were collected in cryovials and frozen for transport for possible metabolomic or single-cell genomic work in the future.

Hole BT1B

A whole-round serpentine sample was collected from Core 39Z in Hole BT1B for DNA/RNA and lipid extractions. Samples were taken from the inside and outside of the core.

- 3 replicates from inside of core (~0.25–0.5 g crushed rock).
- 3 replicates from outside of core (~0.25–0.5 g crushed rock).
- The remainder of the core was frozen at –80°C for future sampling needs.

Sites BA1 and BA2

Samples of drill cuttings were taken for DNA/RNA extraction and spectroscopic and bulk nitrogen analysis.

DNA/RNA extraction

Crushed drill cuttings samples were collected at a depth of 54 m.

- 3 replicates (~0.25–0.5 g crushed rock).
- 2 replicates of drilling foam/liquid (~20 mL).
- An additional 3 replicates of crushed drill cuttings were collected in cryovials and frozen for transport for possible metabolomic or single-cell genomic work in the future.

Spectroscopic analysis

- Site BA1: ~15 g of drill cuttings were sampled from every 10 m at 10–140 m depth and every 20 m at 150–390 m depth. Additional samples of interest were also collected at 23, 58, 64, 65, 66, 144, 148, and 400 m depths.

- Site BA2: ~15 g of drill cuttings sampled every 20 m at 3–383 m depth plus 1 sample at 400 m.

Bulk nitrogen analysis

- Hole BA1A: cuttings sampled every 20 m from 130–390 m depth.
- 2 g from the wet-sieved, <2 mm, aerobically prepared fraction of the samples collected above from Hole BA1A for spectroscopic analysis.

Sites BA1, BA3, BA4

During Phase 2 drilling operations, a 50 cm BIO whole-round core microbiology sample was taken once every ~10 m from Holes BA1B, BA3A, and BA4A as described in Microbiology in the **Methods** chapter. Microbiology subsamples were allocated from BIO whole-round samples as follows:

- DNA extraction and sequencing: 5 cm intact whole-round.
- Lipid extraction: 15 cm intact whole-round.
- DNA preservation: 4 cm intact whole-round.
- Florescence microscopy, cell counts, tracer counts: <0.5 cm whole round crushed, formaldehyde-fixed.
- Cultivation experiments: <0.5 cm whole round crushed, preserved in anoxic site water.
- Carbon compound transformation rates: 5 cm intact whole round.
- Raman, electron probe, XANES, C-imaging, XRD, S-isotopes: 4 cm intact whole round.
- TOC, TIC, and carbon isotopes: 1 cm intact whole round.

Results

16S amplicon sequencing of DNA

Subsurface fluids and rocks are known to contain microbial life to great depths, with temperatures >150°C often considered an upper limit. During Phase 1, we utilized a few small sections of gabbro (Site GT3) and listvenite (Site BT1) core to test our ability to successfully extract DNA and amplify and sequence genes of interest using well-established kits and protocols. We have a significant amount of data regarding the microbial communities that can be detected in gabbro and peridotite-hosted fluids in Oman, and thus we can compare any preliminary data from Sites GT3 and BT1 to those data sets to look for overlaps or any suggestions of novel lineages within the rock vs. fluid phase.

Sample contamination

Successful extraction and sequencing of DNA and cDNA (from RNA) from crushed rock samples at very low concentrations was achieved. Whereas contamination is an important factor (e.g., from drill fluids and human contact), we are able to pull out sequences that correspond to some interesting microorganisms from "candidate divisions" and oligotrophic lineages. Microbial candidate divisions are groups of organisms that have been identified in environmental sequencing but for which no cultured example exists. Once grown and characterized in a laboratory setting for its physiological properties, a division can be named and is no longer a candidate. These candidate divisions are often difficult to isolate from their environment, and genomic information can be useful in achieving that goal. We have seen a number of candidate bacterial phyla in very low abundances in the crushed rock samples, including Acetothermia (OP1). Other noted candidate groups include OP3, OP5, OP8, OP9, OP10, OP11, and OD1. Additionally, microbial groups previously found in the arctic subseafloor, a gold mine, and other diverse environments are noted in very low abundances. Work is ongoing to identify and learn about these microorganisms and further filter out contamination. This is all exciting news from these samples, as a push is on in the environmental microbiological and geobiological worlds to better understand the role and function of organisms that are present in trace amounts, the so-called "microbial dark matter" found in most environments. That we are finding good potential in samples from Oman hints at new understanding for the future of what is known of the evolutionary Tree of Life.

The following amounts of DNA were recovered from rock samples (assuming ~5 fg of DNA per cell):

- Hole BA1A cuttings (54 m depth): <0.17–31.7 ng DNA/g rock (<3.4×10^4 to 6.33×10^6 cells/g rock).
- Site GT3 (inner core): <0.17 ng DNA/g rock (<3.4×10^4 cells/g rock).
- Site GT3 (outer core): <0.17 ng DNA/g rock (<3.4×10^4 cells/g rock).
- Hole BT1B (inner core): <0.17 ng DNA/g rock (<3.4×10^4 cells/g rock).
- Hole BT1B (outer core): <0.17–20.33 ng DNA/g rock (<3.4×10^4 to 4.07×10^6 cells/g rock).

Cell estimates above are based on DNA yields postextraction, so these numbers do not account for cells and DNA lost during the extraction process. These data are in general agreement with some previous Integrated Ocean Drilling Program (IODP) findings: IODP Expedition 337 cell counts indicated <10^6 cells/cm^3 from cuttings, most all of which was attributed to contamination from drilling mud. If we use a density of 3 g/cm^3 for basalt rock, that is 3.3×10^5 cells/g rock. Using microscopy and flow cytometry, cell counts on core samples from Expedition 337 showed cell numbers were generally 10^2–10^4 cells/cm^3 of rock, equivalent to 33.3 to 3.3×10^3

cells/g basalt, decreasing with depth (see figure F60 in Expedition 337 Scientists, 2013).

We also conducted tests on DNA extraction from the Hole BA1B well chips (Fig. F1). However, it appears that most of the DNA from the chips originate from the foam and human contact. Currently, we do not intend to utilize well chips for DNA and lipid analyses given the extent of surface contact with the drilling fluids.

Bar charts are often used to visualize microbial abundances from a sampling event. In Figure F2, each sample was taken in triplicate (e.g., BA1.1, BA1.2, BA1.3, as a sampling event) and split into DNA and RNA fractions (hence the RNA1, RNA2, etc., labels). A full bar in the graph represents the extracted microbial community, with each color representing a different taxonomic group of microorganisms (an Order). Information on general metabolic functionality and habitat requirements of these microbial groups can often be inferred based on this classification if a group has been previously identified and studied. Larger single colors within a bar indicate a greater percentage of the total community is attributed to one microbial group. In Sample BA1.RNA1, for example, most of the bar is orange, indicating most of the sampled microbial community belongs to the taxonomic Order Flavobacteriales. The distribution of microbial abundances between samples can also provide information on microbial ecology in the subsurface.

The combined field and laboratory DNA/RNA extraction protocol used in 2017 works and can be improved. Some easy changes that would help reduce contamination during core collection, preparation, and processing are as follows:

- All core handlers should wear nitrile gloves.
- Flame sterilize the outside of a piece of core dedicated to DNA extractions prior to wrapping in sterile aluminum foil.
- Crush and process larger masses of rock per sample to increase yield and quality of results. This mass increase does not necessarily require more whole-round material than the 5 cm lengths we received, but the extraction protocol could be altered slightly to allow for greater mass input.
- Use a hydraulic core splitter to greatly aid paring the potentially contaminated outer core, allowing collection of uncontaminated inner core with speed and ease to obtain gram amount samples for DNA/RNA/cultivation.
- Continue to sample drilling fluids, washing water, and other contamination controls.

Bulk $\delta^{15}N$ analysis of well chips (Hole BA1A)

In addition to bulk nitrogen isotope analysis, as described in Microbiology in the **Methods** chapter, bulk dissolved and exchangeable nitrogen species in well chips were analyzed in a pore water leachate, as described here. To prepare the pore water leachate, ~1 g of the sieved and washed sample was added to acid-washed polypropylene tubes containing 5 mL of organic-free water. Tubes were incubated at 30°C and shaken at 250 rpm for 1 week. After the incubation period, tubes were centrifuged and supernatant was collected in a clean tube and frozen. The remaining sample was air-dried and then crushed to a fine powder using an agate mortar and pestle. The powdered sample was transferred to a clean tube with 5 mL organic-free water and incubated again at 30°C and shaken at 250 rpm for 1 week to measure dissolved nitrogen species in fluid inclusions. Once again, at the end of the incubation period, supernatant was collected and frozen.

To measure exchangeable N, 5 mL of 1 M potassium chloride was added to the same tube. Samples were incubated overnight and the supernatant from this incubation was collected and frozen. Dissolved nitrate and nitrite from each of the three incubations were measured via spectrophotometry on a Biotek Synergy H1 microplate reader using the protocols described in Garcia-Robaldo et al. (2014). Ammonium concentrations were also measured through microplate colorimetry using protocols adapted from Weatherburn (1967).

To measure the bulk dissolved nitrogen concentration from pore water leachate and fluid inclusions, 1 mL of supernatant was oxidized with 1 mL of persulfate solution (2 g organic cleanly reprecipitated potassium persulfate and 2 g Optima grade sodium hydroxide in 100 mL Savillex water) during a 120 min autoclave incubation. Oxidized samples (all N converted to dissolved nitrate) were then pH adjusted to neutral and quantified by conversion to NO followed by chemiluminescence detection (Braman and Hendrix, 1989) on an Antek1750 nitrate/nitrite analyzer. Then, 20 nmol of measured nitrogen was denitrified using *P. chloraphis* (Weigand et al., 2016) to nitrous oxide for measurement on a gas chromatograph–infrared mass spectrometer (GC-irMS; Thermo MAT 253) with an N_2O extraction and purification system at Princeton University.

To measure bulk rock nitrogen, ~2 g of the sieved and washed sample was crushed to a fine powder using an agate mortar and pestle. A 400–600 mg subsample of powder from each sample was weighed into 9 mm × 10 mm tin capsules, sealed, and then introduced in the autosampler of a Thermo Delta V with elemental analyzer for continuous flow analysis of bulk rock nitrogen stable isotopes. Samples contained very little nitrogen, and so tin capsule blanks were run after each sample to allow for precise blank corrections.

Well chip samples were found unsuitable for bulk $\delta^{15}N$ measurements due to contamination with or-

ganic nitrogen from drilling fluid and foam. The measured concentration of total N (after persulfate oxidation) from pore water leach and fluid inclusion protocols was ~7 times greater than the combined concentration of measured nitrate, nitrite, and ammonium, despite washing the well chips prior to the incubation and procedural blanks having nitrogen concentrations below the detection limit of the methods. This high concentration of detected organic N, even in fluid inclusion samples that had previously been subjected to a week-long incubation in organic-free fluid prior to crushing, suggests the drilling foam or fluid must have penetrated the interior of the well chip and attached to mineral surfaces, as it was not completely removed during washing. Accordingly, powdered rock samples for bulk analysis would also be extremely contaminated. Because the signal from this contamination is far greater than the signal from ammonium sourced from the rock itself, we could not reliably subtract the isotopic signal from contamination.

The pervasive contamination of well chip samples with organic material observed during the attempt to quantify bulk nitrogen in well chips necessitates a more comprehensive sampling of potential sources of contamination for lipid analysis. The quantification of lipid and hydrocarbon compounds from drilling mud and water, the core barrel, trays, and saw in contact with the core prior to subsampling, as well as the air on the drill site, should allow for subtraction of these contaminating compounds from those detected in the interior of the rock core. A wash with Milli-Q water on site prior to transportation of these samples should also prevent the penetration of contaminants on the exterior of the core into the pristine interior.

Without these contamination controls, we cannot confidently assess what organics extracted from the rock core are autochthonous.

Microscopic and spectroscopic analysis of well chips

We conducted preliminary microscopic and spectroscopic analysis of well chips recovered during rotary drilling in Hole BA1A in order to determine how changes in Fe- and S-bearing primary and secondary phases vary as a function of depth. This information is critical for developing hypotheses regarding how microbial activity may be directly influencing mineral transformations during low-temperature serpentinization.

Microscopic examination of thin sections prepared from drill cutting materials from Hole BA1A was conducted at 20 m intervals between 10 and 390 m depth. Across all depths, the majority of grains were dominated by mesh-textured serpentine after olivine, sometimes with variable amounts of brucite, olivine, pyroxene, and chromite. Bastite textures (serpentine after orthopyroxene) were also frequently observed in association with mesh-textured serpentine. There were frequently other rock fragments, or portions of fragments, that were mostly colorless in thin section, often with fibrous texture. The colorless fragments examined each contained a mixture of some subset of the minerals diopside, talc, amphibole, clinochlore, garnet, and xonotlite. Still other chips contained a mottling of different textures, including mesh-textured serpentine, large pyroxene crystals, and colorless regions with fibrous texture. Examples of these three types of chips are shown in Figure F1.

Samples collected very near the surface had clear differences from deeper samples. The 10 m sample, which represents alluvium, was dominated by oxidized orange serpentine; some relict olivine and pyroxene were also present. Based on Raman spectroscopy, the orange staining was attributed to the presence of both hematite and goethite intermixed with serpentine. The 30 m sample, which was below bedrock, appeared very heterogeneous with some chips having orange-colored serpentine and others with a notable opaque overprinting associated with mesh texture rims as well as cores.

Samples from 50–250 m contained variable amounts of the same opaque overprinting observed in some grains of the 30 m sample. The opaques peak in abundance at ~70 m depth and then decrease with greater depth. The opaque phases were often limited to mesh cores but were also observed in mesh rims. Raman spectra collected from the opaque material were consistent with a sulfide mineral in many cases, although magnetite is present as an opaque mineral as well. Sulfide minerals are generally characterized by several bands at low Raman shifts (100–400 cm^{-1}), but uniquely identifying specific sulfide minerals based only on the Raman spectrum is often difficult. Wavelength dispersive spectroscopy (WDS) mapping of these areas showed that sulfur is present with the opaque material, corroborating that these are sulfide minerals. Brucite was also identified in many of the mesh cores containing sulfides.

We transported several of these samples to the Stanford Synchrotron Radiation Lightsource in order to determine more about the Fe speciation and oxidation state in these samples. In particular, we are focusing on redox gradients and mineralogical transformations surrounding Fe-rich brucite cores. We are also further interrogating the opaque phases to determine the abundance of sulfide and magnetite. The extensive formation of sulfide is of great interest to our microbiological studies, where we are investigating biologically mediated processes such as sulfate reduction coupled to the oxidation of hydrogen, formate, or methane, resulting in the formation of secondary Fe and Ni sulfides.

Mineralogical characterization of subcores

We conducted microscopic examinations and mineralogical characterizations on 52 subsamples from whole-round cores (WRC) designated for microbiological analyses. These observations provide a crucial context for targeting and identifying mineralogical controls on microbiological distribution and activity in this heterogeneous rock-hosted environment.

We examined petrographic thin sections to understand the range of lithologies, mineralogic associations, and alteration histories represented in the BIO WRC sample set from Holes BA3A, BA1B, and BA4A. Simplified stratigraphic columns indicating lithology and sample locations are included in (Fig. F3). The lithologies of the samples investigated so far are composed of serpentinized harzburgite and dunite with some veins of rodingitized gabbro and diopsidite and talc-amphibole assemblages. In general, these rocks have undergone multiple generations of serpentinization, evidenced by complex networks of crosscutting veins that often contain different polymorphs and generations of serpentine.

In all three boreholes, the first BIO sample obtained at ~10 m depth was within the weathered, near-surface environment and contained Fe oxides (frequently goethite, and also hematite). Carbonate minerals (dolomite and aragonite) were also observed in the 10 m thin section from Hole BA4A, whereas dolomite was detected in the X-ray diffraction (XRD) pattern for samples from Hole BA1B at 5 and 10 m. Carbonate minerals have not been detected in the other BIO samples investigated thus far. The oxidized appearance of the samples diminishes quickly, and by 20 m depth the serpentine is green and magnetite is the only Fe oxide observed.

The serpentinized dunite and harzburgite generally exhibit mesh and bastite alteration textures after olivine and orthopyroxene, respectively. Within these serpentinized peridotites we have identified olivine, orthopyroxene, clinopyroxene (diopside), serpentine (mainly lizardite with some chrysotile), chromite, brucite, magnetite, chlorite, garnet, metal sulfides, and occasional amphibole (tremolite-actinolite) and xonotlite ($Ca_6Si_6O_{17}[OH]_2$). Quantitative powder XRD results are shown in Figure F3 for the major mineral components that could be detected by XRD. The finely dispersed, opaque metal sulfides are common in mesh cores in Hole BA1B from ~40 to 200 m and in Hole BA4A below ~50 m but are not encountered in Hole BA3A (Fig. F4). Though these sulfides are widespread, we have not yet been able to identify the sulfide minerals present or their formulae, and they could not be robustly detected in XRD patterns, suggesting that they may be amorphous or the overall bulk abundance may be low. The sulfide is typically dispersed in Fe-bearing brucite and/or serpentine (lizardite and chrysotile), which can be identified by Raman spectroscopy (Fig. F5).

In many samples there are millimeter-scale colorless serpentine (chrysotile and lizardite) veins that crosscut almost everything and appear very late. These sometimes bear garnet but not magnetite.

Gabbro veins have been rodingitized, with plagioclase fully replaced by a fine-grained mixture of serpentine, chlorite, garnet, and sometimes xonotlite. Typically, clinopyroxene appears largely unaltered, olivine is replaced by mesh-textured serpentine, and plagioclase is replaced by a fine-grained mixture of serpentine, chlorite, and garnet.

Fe redox and the role of brucite

Abundant Fe-bearing brucite has been identified in the Site BA core samples. Brucite is widespread throughout the BA cores, and the abundance reaches 6–8 wt% in the most brucite-rich samples (Fig. F3). Optical microscopy and Raman spectroscopy reveal that brucite is often localized within mesh cores where olivine has been fully replaced. In cores from Holes BA1B and BA4A, these cores frequently contain a mixture of brucite and the finely dispersed, opaque metal sulfides. In Hole BA3A, these cores contain relatively pure Fe-rich brucite. Additionally, brucite can be found finely intergrown with serpentine mesh rims and veins. Based on variations in the Raman spectrum of brucite (the position of the OH-stretch peak), it ranges from Fe rich to Fe poor, even at the microscale within a thin section as shown in Figure F6.

Two trends in brucite abundance can be distinguished in Figure F3 and confirmed by optical microscopy and Raman spectroscopy. First, although brucite can be abundant in harzburgite, it is generally more abundant in dunite. This is expected since the serpentinization of orthopyroxene in harzburgite releases excess silica, which reduces the amount of brucite formed from olivine hydration in favor of serpentine. Second, the abundance of brucite is reduced in all three cores shallower than ~100 m depth. This may reflect more recent breakdown of brucite during modern water-rock interactions, which is of direct interest for identifying zones for localized energy generation and potential microbial activity.

To further investigate whether brucite may be currently participating in modern reactions, we examined samples above and below 100 m depth in Hole BA3A because the absence of metal sulfides associated with brucite significantly simplifies measurements of brucite Fe content. The sample from 300 m in Hole BA3A contains abundant brucite in mesh cores, and quantitative WDS mapping by electron microprobe analysis (EMPA) reveals that this brucite contains as much as 15–20 mol% substitution of Fe for Mg ($Fe/(Fe + Mg) = X_{Fe} = 0.15–0.20$). This is confirmed by Raman spectroscopy, where the position

of the OH-stretch peak has been calibrated for Fe and is sensitive only to Fe substituted into the brucite structure, as opposed to minor serpentine or other Fe-bearing phases that may contribute to mixed analyses by EMPA. Brucite in the 300 m sample from Hole BA3A gives an X_{Fe} value of 0.16 ± 0.05 by Raman spectroscopy.

In contrast, the sample from 100 m depth in Hole BA3A contains little brucite and mesh cores are replaced with serpentine. Quantitative WDS mapping reveals that these mesh cores can contain a similar amount of Fe substitution to the brucite (X_{Fe} = 0.15–0.20). This is quite Fe rich for serpentine and suggests that this serpentine may have replaced preexisting brucite with conservation of Fe in a reaction that would require addition of SiO_2 from the fluid. The redox state of Fe in this Fe-rich serpentine is not yet known and is a target for investigation in the near future.

Characterization of garnet

Garnet was found to occur as a widespread minor component across all lithologies. Garnet also occurs in many distinct textural contexts. Garnet is abundant in the fine-grained serpentine-chlorite-garnet assemblage replacing plagioclase in rodingitized gabbro and also frequently associated with diopsidite veins, bastite serpentine, serpentine mesh texture, and late serpentine veins. The garnet is often very fine grained and found in a serpentine or xonotlite matrix (Fig. F7).

Because garnet could record low-temperature alteration processes, EMPA was used to determine the garnet chemistry and approximate water content on a subset of samples displaying the various textural garnet occurrences. All analyzed garnets were hydrous andradite-grossular in composition. Garnet replacing plagioclase within the rodingitized gabbro (sample from 250 m in Hole BA1B [BA1B-250 m]) was the most hydrous and the most Al^{3+} rich of all garnets observed, with the average formula (hydrogrossular)

$$Ca_{3.03}Fe^{3+}_{0.61}Al_{1.37}(SiO_4)_{2.20}(OH)_{3.16}. \quad (1)$$

Garnets associated with serpentinized peridotite—occurring within bastite serpentine (Hole BA3A, 170 m), serpentine mesh (Hole BA1B, 140 m), and late-stage serpentine veins (Holes BA3A, 60 m; BA1B, 140 m)—were more andraditic in composition with a significant hydrous component and average formula

$$Ca_{3.07}Fe^{3+}_{1.68}Al_{0.23}(SiO_4)_{2.66}(OH)_{1.29}. \quad (2)$$

Hydroandradite in other serpentinizing systems has been interpreted as a sign of low-temperature alteration, especially when it has been found in paragenesis with polyhedral serpentine (Ménez et al., 2012, 2018; Plümper et al., 2014). Andradite may form under strongly reducing conditions, and the incorporation of Fe(III) is likely to accommodate hydrogen production. We examined two occurrences of hydroandradite in late-stage serpentine veins (Holes BA3A, 60 m; BA1B, 140 m) by transmission electron microscopy (TEM) to determine whether polyhedral serpentine was present in contact with hydroandradite. The serpentine in contact with hydroandradite in Sample BA3A-60 m was extremely fine grained, and no positive determination of the serpentine structure could be made. However, polyhedral serpentine was identified in Sample BA1B-140 m in contact with hydroandradite, indicating that the vein was formed during reaction at <230°C.

Biological sulfate reduction rates

Dissimilatory sulfate reduction (SR) is among the oldest known microbial processes on Earth and it is the predominant anaerobic microbial process in sulfur-rich marine sediments (Canfield and Raiswell, 1999). Recent measurements revealed that sulfate is available in several of the water-bearing rocky environments now known beyond Earth, making SR a potentially important metabolism in those systems (Vance et al., 2016). The inferred presence of both sulfate and peridotite rocks in ophiolites points toward a potential niche for sulfate reducers and highlights the need to understand how and under which conditions SR occurs in serpentinizing systems on Earth.

We conducted assays to measure the potential rate of biological sulfate reduction in the partially serpentinized and sometimes partially sulfurized WRC subsamples collected by the BIO team. Twenty three "G" samples have been used so far from Holes BA3A, BA1B, and BA4A, and they were selected to contrast potential biological activity as a function of depth and mineralogical characteristics.

We detected microbial sulfate reduction in almost all cores at low rates in the range of 3–800 fmol/cm^3/d. In most of the samples, amendment of H_2 or CH_4 resulted in a slight increase of the turnover rates by a factor of 2–3 (Fig. F8). Highest rates were found in the deeper cores of Holes BA1B and BA4A. For example, in Hole BA1B a maximum was found at 280 mbs (meters below surface) target depth, and in Hole BA4A the maximum sulfate reduction rate was found at 230 mbs. The uppermost samples of Holes BA1B and BA4A, as well as most depths of Hole BA3A, exhibited very low sulfate reduction rates that were often only detectable in the samples amended with H_2 or CH_4. It appears that the samples where highest sulfate reduction rates were found correspond to depth zones with lower pH (alkaline conditions, pH 9–10) and most negative redox potential of the pore

fluids. A deeper analysis of the data set and comparison with mineralogical composition and, for example, the presence of veins will follow in the future.

Interestingly, the killed control samples also showed sulfate turnover to a small extent. Although this turnover was generally significantly lower than in the biological samples, this result is unexpected. Abiotic sulfate reduction at temperatures <100°C or more is not known. The turnover of sulfate may be due to very robust microbial endospores that survived the incubation treatment and may have germinated during preincubation and incubation, but this possibility will need to be further tested.

References

Braman, R.S., and Hendrix, S.A., 1989. Nanogram nitrite and nitrate determination in environmental and biological materials by vanadium(III) reduction with chemiluminescence detection. Analytical Chemistry, 61(24):2715-2718.

Expedition 337 Scientists, 2013. Site C0020. In Inagaki, F., Hinrichs, K.-U., Kubo, Y., and the Expedition 337 Scientists, Proc. IODP, 337: Tokyo (Integrated Ocean Drilling Program Management International, Inc.). https://doi.org/10.2204/iodp.proc.337.103.2013

Canfield, D.E., and Raisewell, R., 1999. The evolution of the sulfur cycle. Am. J. Sci., 299:697-723.

Garcia-Robledo, E., Corzo, A., Papaspyrou, S., 2014. A fast and direct spectrophotometric method for the sequential determination of nitrate and nitrite at low concentrations in small volumes. Mar. Chem., 163:30-36.

Ménez, B., Pasini, V., and Brunelli, D., 2012. Life in the hydrated suboceanic mantle. Nat. Geosci., 5:133–137.

Ménez, B., Pasini, V., Guyot, F., Benzerara, K., Bernard, S., and Brunelli, D., 2018. Mineralizations and transition metal mobility driven by organic carbon during low-temperature serpentinization. Lithos, 323:262-276. https://doi.org/10.1016/j.lithos.2018.07.022

Plümper, O., Beinlich, A., Bach, W., Janots, E., and Austrheim, H., 2014. Garnets within geode-like serpentinite veins: implications for element transport, hydrogen production and life-supporting environment formation. Geochim. Cosmochim. Acta, 141:454–471.

Vance, D., Little, S.H., Archer, C., Cameron, V., Anderson, M.B., Rijkenberg, M.J.A., Lyons, T.W., 2016. The oceanic budgets of nickel and zinc isotopes: the importance of sulfidic environments as illustrated by the Black Sea. Phil. Trans. Royal Soc. A: Mathematical, Physical, and Engineering Sciences, 374(2081).

Weatherburn, M.W., 1967. Urease-Berthelot colorimetric method for in vitro determination of urea. Analytical Chemistry, 39:971-974.

Weigand, M.A., Foriel, J., Barnett, B., Oleynik, S., Sigman, D.M., 2016. Updates to instrumentation and protocols for isotopic analysis of nitrate by the denitrifier method. Rapid Communications in Mass Spectrometry, 30(12):1365-1383.

Figure F1. Transmitted light micrographs of drill cuttings from Site BA1 in thin section. Opaque sulfide overprinting from 50 m depth concentrated in (**A**) mesh cores (plane polarized light [PPL]) and in (**B**) mesh rims (PPL). **C, D.** Colorless, fibrous texture fragment from 50 m depth (C: PPL, D: cross-polarized light [XPL]. **E, F.** Mottled serpentine mesh, diopside, and fibrous texture from 370 m depth (E: PPL, F: XPL).

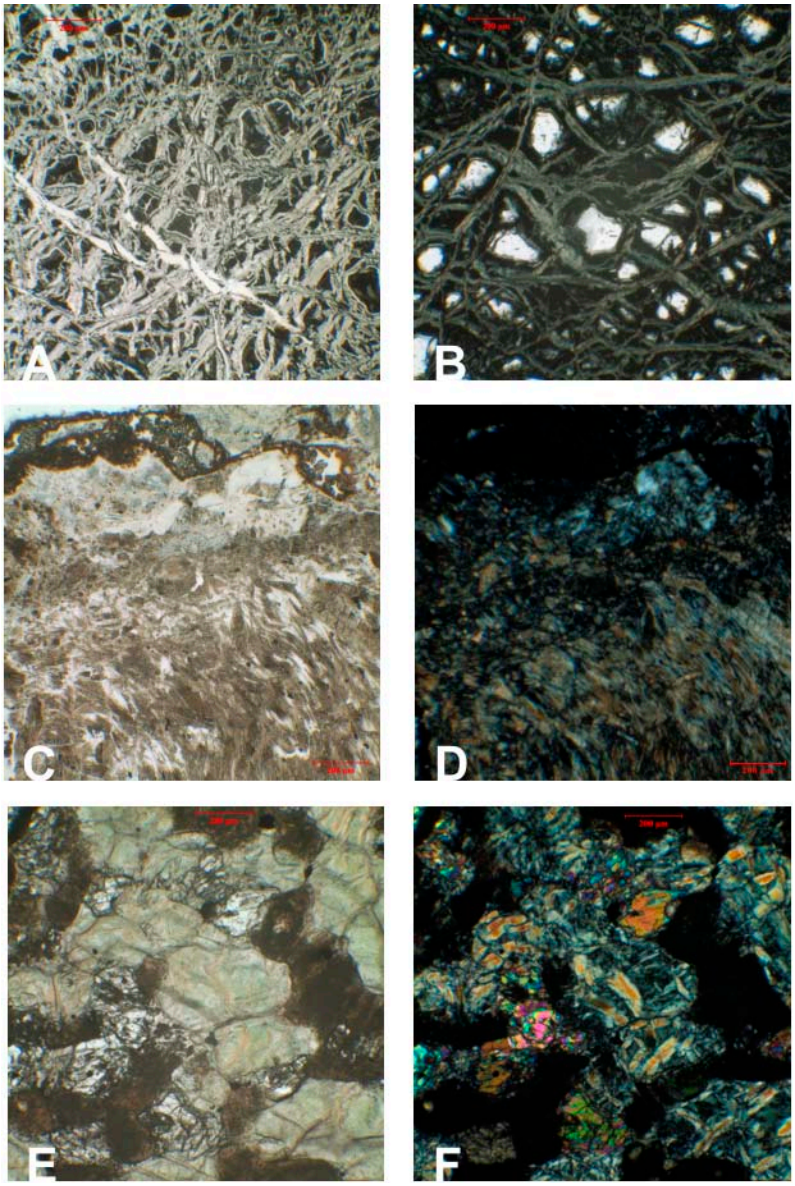

Figure F2. Relative abundance of microbial orders present in 2017 rock samples. Well chips from 54 m depth and drilling fluid/foam were collected from Site BA1. Hole BT1B serpentine inner and outer core (named BT1BCont.) were collected as well as inner and outer core samples from Site GT3 gabbro. Fluid from the rock saw used to cut GT3 cores was sampled (RSawWat.) as an additional contamination control.

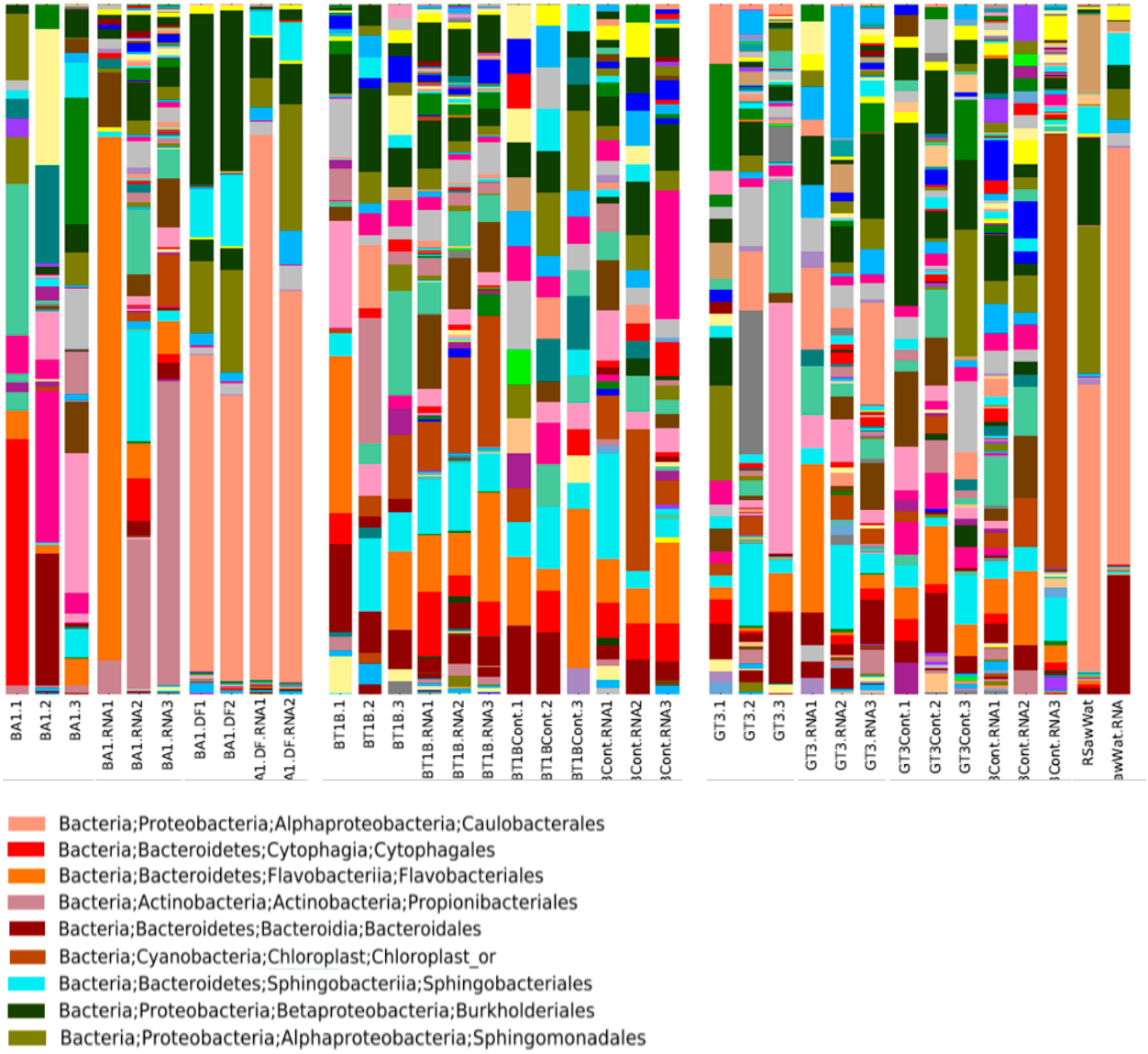

Figure F3. Quantitative powder XRD results for the major mineral components that could be detected by XRD.

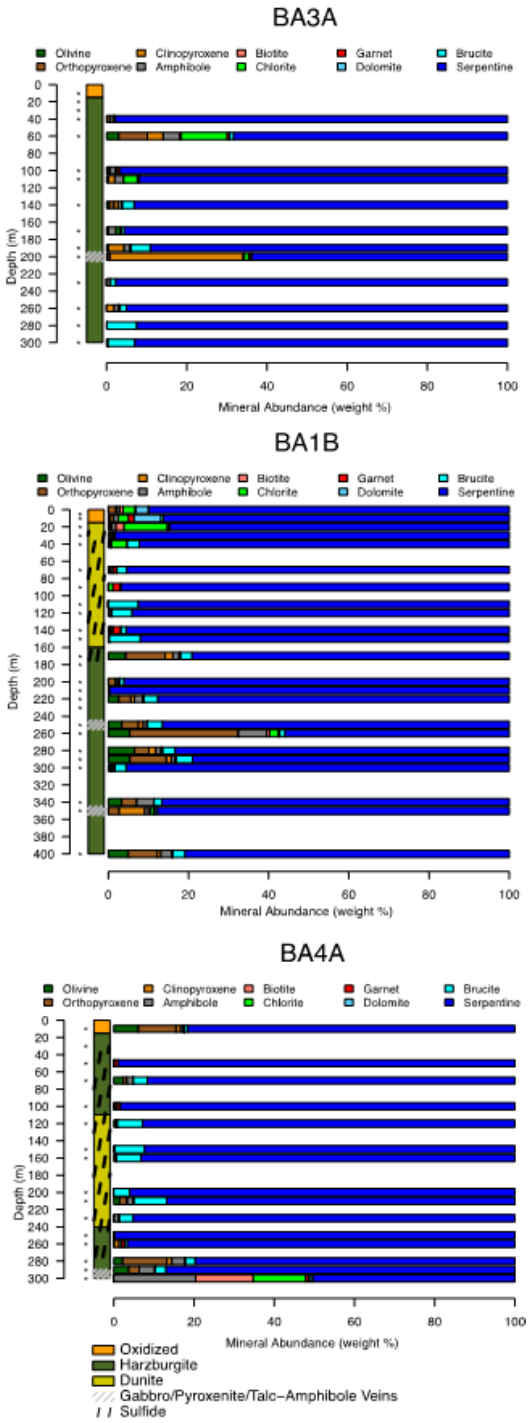

Figure F4. Finely dispersed opaque metal sulfides are common in mesh cores in Hole BA1B at ~40–200 m and Hole BA4A below ~50 m but are not encountered in Hole BA3A.

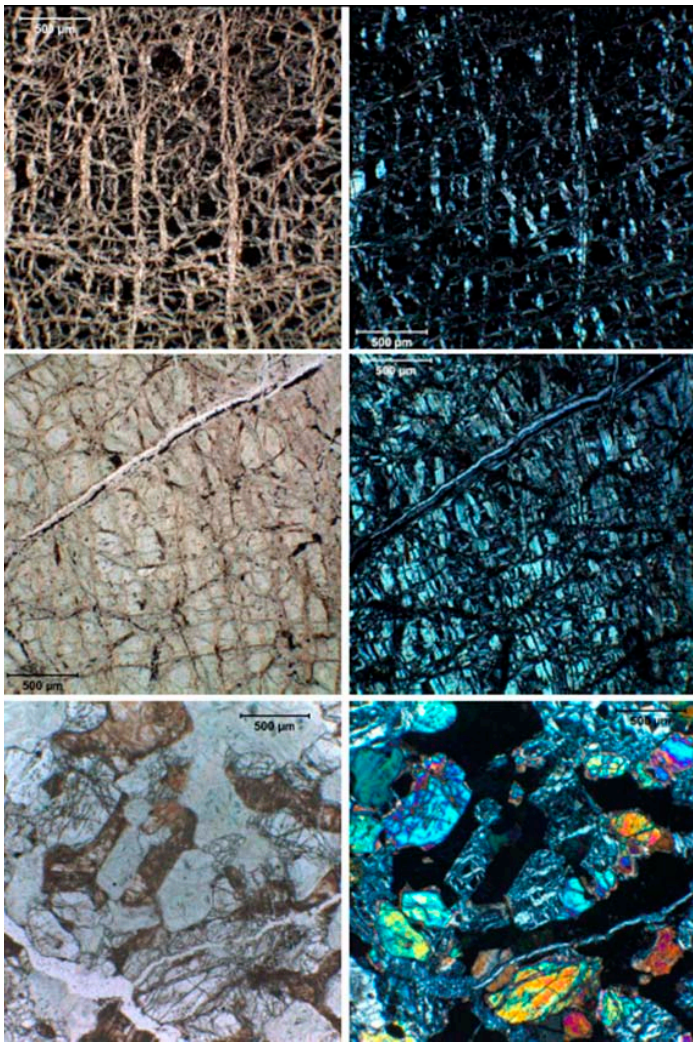

Figure F5. Though these sulfides are widespread, we have not yet been able to identify the sulfide minerals present or their formulae, and they could not be robustly detected in XRD patterns, suggesting that they may be amorphous or the overall bulk abundance may be low. The sulfide is typically dispersed in Fe-bearing brucite and/or serpentine (lizardite and chrysotile), which can be identified by Raman spectroscopy.

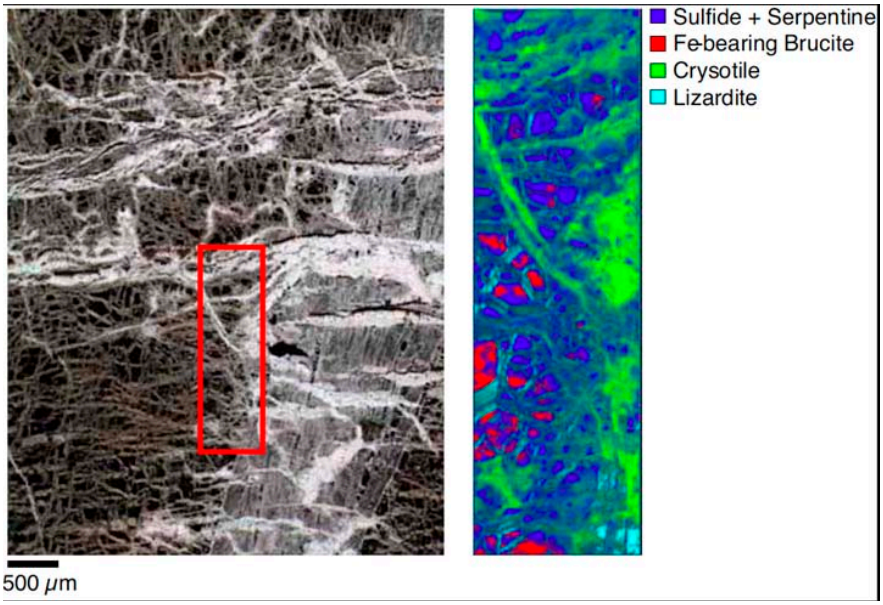

Figure F6. Based on variations in the Raman spectrum of brucite (the position of the OH-stretch peak), it ranges from Fe rich to Fe poor, even at the microscale within a thin section.

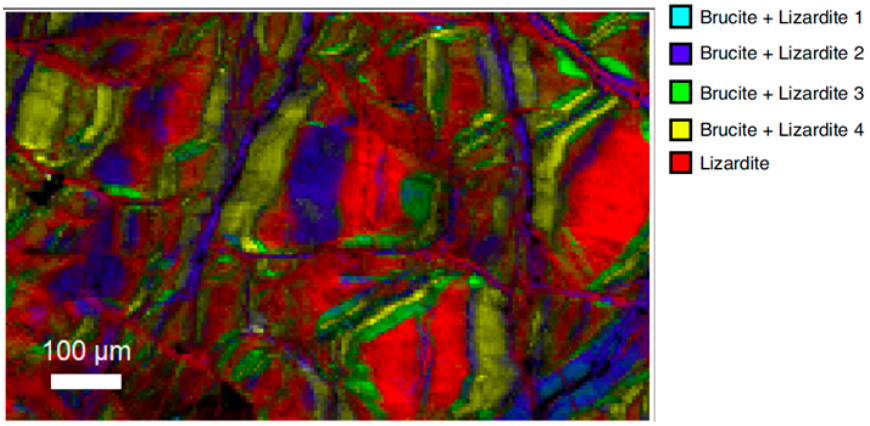

Figure F7. Garnet is often very fine grained and found in a serpentine or xonotlite matrix.

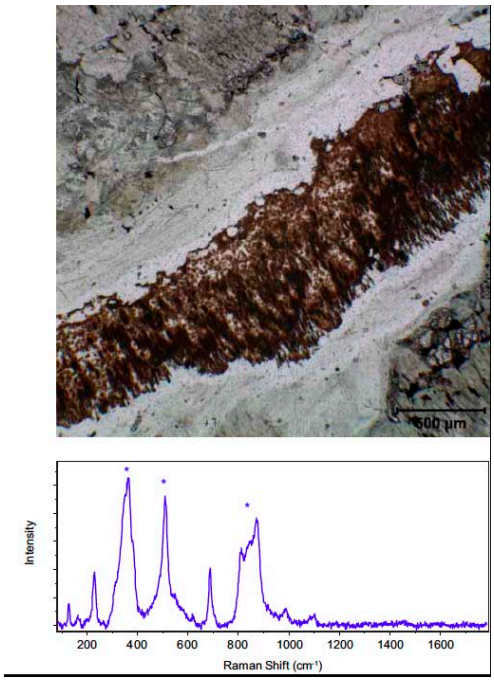

Figure F8. In most of the samples, the amendment of H_2 or CH_4 resulted in a slight increase of the sulfate reduction turnover rates by a factor of 2–3.